Eur. J. Mech. B/Fluids, **18**, n° 2, 213-226, 1999

Viscous shock layer on a plate in hypersonic flow

A.A. MASLOV *, S.G. MIRONOV, T.V. POPLAVSKAYA, A.N. SHIPLYUK, V.N. VETLUTSKY

ABSTRACT. – The results of theoretical and experimental investigations of the hypersonic flow around a plate with a shap leading edge are presented. Step-by-step verification of the numerical model of the full viscous shock layer is performed: the calculated density profiles, shock wave inclinations, and the Stanton numbers are compared with experimental data obtained using the method of electron-beam fluorescence, calorimetric gages and IR imaging system. © Elsevier, Paris.

1. Introduction

The development of numerical methods considerably decreases the time and cost of experimental research into complex flows; it makes it possible to obtain the overall field of gas dynamic parameters of the flow and to perform wide-scale parametric investigations of the process under study. Numerical methods have irrefutable advantages for predicting the flow characteristics under the conditions of high-enthalpy flow when the measurement of individual parameters of the flow field presents a complicated technical problem.

In the mathematical simulation of physical processes, the source model inevitably has some simplifications based on the current concept of dominating mechanisms of a phenomenon and their relationship. The process of identification of mechanisms and relationships requires a qualitative and quantitative comparison of the calculated results with the data of wind tunnel or flight experiments. The test objects are generally fairly simple, canonical types of flow that help to reveal the essential features of the phenomenon under investigation.

A widely used test object for verification of numerical methods is the flow on a plate with a sharp leading edge. At hypersonic flow speeds and moderate Reynolds numbers, a wide range of flow regimes, classified in McCroskey et al. (1966), Poplavskaya and Vetlutsky (1997), is formed even on such simple models. There is a small free-molecular region directly on the leading edge, then follows a transitional region (merged layer) where the boundary layer and the shock wave interact and merge to such an extent that it is not possible to draw a distinct line between them. This region asymptotically transforms into a strong interaction region where the parameters behind the shock wave can be calculated using the generalized Rankine-Hugoniot conditions. A weak interaction regime is observed further downstream, where the boundary layer is distinguished as a separate flow region.

The known experimental works (McCroskey et al., 1966; Lengrand et al., 1992; Harbour and Lewis, 1967; Metcalf et al., 1969) for Mach numbers higher than 10 deal with the flow on a plate at zero incidence and low Reynolds numbers ($\mathrm{Re}_x \sim 10^3$, where Re_x is the local Reynolds number based on the free stream parameters) corresponding to the merged layer region. There are no measurement data now for the higher Reynolds numbers which are of interest, for example, for the flow stability problem. It should be noted that

* Correspondence and reprints.
Institute of Theoretical and Applied Mechanics, Russian Academy of Sciences, Siberian Branch, 630090, Novosibirsk, Russia.
E-mail: maslov@itam.nsc.ru

0997-7546/99/02/© Elsevier, Paris

experimental investigations of hypersonic flow parameters are very complicated, and the same accuracy cannot be ensured here as at supersonic speeds.

Theoretical investigations of the hypersonic flow past a flat plate of Cheng (1961), Cheng et al. (1961), Pan and Probstein (1966), Shorenstein and Probstein (1968), Rudman and Rubin (1968) are mainly devoted to the merged layer region with local Reynolds number lower than 10^4. Pan and Probstein (1966), however, present the correlation formulas for pressure and heat transfer on the plate surface for air both in the merged layer and in the strong interaction region. For the Stanton number this formula looks like:

$$St_{SI} = (0,368T_W/T_0 + 0,0684)[M_\infty \sqrt{C/\mathrm{Re}_x}]^{3/2}. \tag{1}$$

The relations for shock position, pressure and heat transfer on the plate surface at incidence have been obtained by Cheng et al. (1961) in the frame of a locally-similar approximation and thin shock layer approximation. These relations, known as Cheng's theoretical data, are frequently cited in the literature. In Wallace and Burke (1965) experimentally measured heat fluxes St and skin friction coefficients C_f on a plate at zero incidence are compared with the corresponding theoretical data derived for various low-temperature regimes (free-molecular regime, strong and weak viscous interaction). The problem of hypersonic viscous interaction on slender bodies with a sharp leading edge has been considered by Rudman and Rubin (1968) using a system of equations that describe the boundary layer, shock wave structure, and inviscid flow core. Though the main attention has been paid to the merged layer region, the suggested theory, in the authors' opinion, is also applicable for the beginning of the strong interaction region.

The objective of the present work is to study hypersonic flow around a plate within the framework of the FVSL model over a wide range of governing parameters and to present results in the form of universal dimensionless relations as functions of the angle of attack, Reynolds and Mach numbers.

2. Numerical study in the framework of the FVSL model

2.1. Justification of the FVSL model

Several approaches to solving the problem of the calculation of hypersonic flow around a pointed body are possible: numerical solution of the Navier-Stokes equations, the boundary layer equations in the second approximation, and the viscous shock layer equations initially suggested by Cheng (1961). At high Mach numbers ($M_\infty \geq 10$) and moderate Reynolds number ($\mathrm{Re}_x \sim 10^4$ to 10^5) the boundary layer thickness is comparable with the shock wave stand-off distance. Thus, a good approximation for such flows is the full viscous shock layer (FVSL) model, which is an intermediate level of asymptotical approximation between the boundary layer equations and the full Navier-Stokes equations. Apart from all terms of the boundary layer equations, the FVSL equations include the conservation equation for momenta projected onto the normal to the plate and all terms of the Euler equations in the hypersonic approximation. The FVSL model, therefore, describes the entire disturbed flow region of viscous gas between the shock wave and the body surface. This model has a certain upstream limit of applicability (like the strong interaction model of McCroskey et al. (1966)), where the boundary layer and the shock wave merge. This occurs at $V = M_\infty \sqrt{C/\mathrm{Re}_x} \approx 0.1$ to 0.15, where V is the rarefaction parameter introduced in McCroskey et al. (1966), C is the Chapman-Rubesin constant. For large V, a merged layer regime is formed.

The full viscous shock layer model has a number of advantages in comparison with other models:

- since there are no second derivatives with respect to the x coordinate in the FVSL equations, it can be solved by the marching method with respect to this coordinate, which allows for a considerable increase in efficiency of computation in comparison with the Navier-Stockes equations;

- the FVSL model allows for calculation of flows with moderately low Reynolds numbers and under the conditions of boundary layer/inviscid gas interaction, which is impossible in the classical boundary layer theory; this model also makes it possible to avoid the problem of searching the external data for the boundary layer;
- the FVSL computations for the whole flow field from the body to the shock wave are performed in the same manner in the regions of both strong and weak interaction.

The viscous shock layer model has been widely used recently in the study of hypersonic viscous flows around blunt bodies (Tirsky and Utjuzhnikov, 1989; Voronkin, 1974; Borodin and Peigin, 1992; Vershinin et al., 1991; Cheng and Emmanuel, 1995). It was shown there that the error of the FVSL equations in comparison with the full Navier-Stokes equations for the pressure, skin friction and heat flux distributions for the flow around blunted cones at moderate Reynolds numbers is less than 1-2%. Cheng and Emmanuel (1995) have shown good agreement between the FVSL equations and the DSMC model for a blunt nose. An algorithm for solving the FVSL equations and the experimental procedure for mean density distribution measurement in a hypersonic flow past a plate with a sharp leading edge at zero incidence are described in Vetlutsky et al. (1995), Poplavskaya and Vetlutsky (1997).

The study of the flow past a plate at incidence allows one to reveal the trend of variation of the flow characteristics due to a considerable change in the Mach number behind the shock wave as the angle of attack is increased, and to determine the applicability limits of the model assumptions. An algorithm for solving the FVSL equations for hypersonic flow past a plate at incidence is presented in Vetlutsky et al. (1997), Maslov et al. (1998).

2.2. Formulation of the problem

Let us write the FVSL equations in the Cartesian coordinate system (x, y) where the x coordinate is directed along the plate surface and y is normal to it. The derivation of these equations is similar to that in the paper by Davis (1970). The Navier-Stokes equations are written in the variables $(x, y\sqrt{\mathrm{Re}_L})$ for the near-wall region and in the variables (x, y) for the external flow. In each of them the expansion with respect to the parameter $1/\sqrt{\mathrm{Re}_L}$ is performed, and the terms up to the second order of this quantity are left. The FVSL equations include all terms of both systems of equations. For convenience in constructing the algorithm of numerical solution of the FVSL equations, one out-of-order term with the second derivative is left in the second equation of motion:

$$
\begin{aligned}
&\frac{\partial \rho u}{\partial x} + \frac{\partial \rho \nu}{\partial y} = 0,\\
&\rho u \frac{\partial u}{\partial x} + \rho \nu \frac{\partial u}{\partial y} - \frac{1}{\mathrm{Re}_L}\frac{\partial}{\partial y}\left(\mu \frac{\partial u}{\partial y}\right) + \frac{\partial P}{\partial x} = 0,\\
&\rho u \frac{\partial \nu}{\partial x} + \rho \nu \frac{\partial \nu}{\partial y} - \frac{4}{3}\frac{1}{\mathrm{Re}_L}\frac{\partial}{\partial y}\left(\mu \frac{\partial \nu}{\partial y}\right) + \frac{\partial P}{\partial y} = 0,\\
&c_p \rho u \frac{\partial T}{\partial x} + c_p \rho \nu \frac{\partial T}{\partial y} - \frac{1}{\mathrm{Pr}}\frac{1}{\mathrm{Re}_L}\frac{\partial}{\partial y}\left(k \frac{\partial T}{\partial y}\right) - \frac{1}{\mathrm{Re}_L}(\gamma-1)M_\infty^2 \mu \left(\frac{\partial u}{\partial y}\right)^2 - (\gamma-1)M_\infty^2\left(u\frac{\partial P}{\partial y} + \nu \frac{\partial P}{\partial y}\right) = 0,\\
&P = \frac{1}{\gamma M_\infty^2}\rho T.
\end{aligned}
\tag{2}
$$

Here u and ν are the velocity components in the x and y directions; P, ρ, μ, k, T are the pressure, density, viscosity, heat conductivity, and temperature, respectively; $\mathrm{Pr} = \mu_\infty c_{p\infty}/k_\infty$ is the Prandtl number; $\mathrm{Re}_L = \rho_\infty U_\infty L/\mu_\infty$ is the Reynolds number based on the free-stream parameters and the model length L. The velocity components in equations (2) are normalized to the free-stream velocity U_∞, the pressure is related to

the doubled dynamic pressure $\rho_\infty U_\infty^2$, viscosity μ, heat conductivity k, specific heat capacity c_p, density and temperature are normalized to their free-stream values, the x and y coordinates are related to the model length L. Exactly these variables are presented in the figures unless specified otherwise. Further parameter transformations are performed in a similar manner to Poplavskaya and Vetlutsky (1997).

It is shown in Poplavskaya and Vetlutsky (1997) that for parameter values $\sqrt{C}M_\infty/\sqrt{\mathrm{Re}_x} > 0.1$ observed in the merged layer and in the region of transition to the strong interaction regime one has to use the slip boundary conditions. Therefore, the slip conditions and the temperature drop are used in the present paper for $\sqrt{C}M_\infty/\sqrt{\mathrm{Re}_x} > 0.1$ (Loitsyansky, 1973), and the usual no-slip conditions and constant surface temperature are employed for lower values.

The shock wave is assumed to be thin, and, to the accuracy of the above approximation, the boundary conditions on the shock wave in deriving the FVSL equations are taken as the generalized Rankine-Hugoniot conditions, which take into account the second-order terms with respect to $1/\sqrt{\mathrm{Re}_L}$, as was done by Magomedov (1970), Tirsky (1975) and Vershinin et al. (1991) :

$$
\begin{aligned}
u_s &= \cos\beta[\cos(\beta+\alpha) + k_s tg\beta \sin(\beta+\alpha)] - \frac{\mu_s \cos^3\beta(1-tg^2\beta)}{\mathrm{Re}_L \sin(\beta+\alpha)}\,\frac{\partial u}{\partial y} \\
\nu_s &= u_s tg\beta - k_s \frac{\sin(\beta+\alpha)}{\cos\beta} \\
P_s &= \frac{1}{\gamma M_\infty^2} + (1-k_s)\sin^2(\beta+\alpha) - \frac{2\mu_s \sin\beta\cos\beta}{\mathrm{Re}_L}\,\frac{\partial u}{\partial y} \\
H_s &= 1 + \frac{\gamma-1}{2}M_\infty^2 - \frac{\cos\beta}{\sigma_s \mathrm{Re}_L \sin(\beta+\alpha)}\left[\frac{\partial H}{\partial y} - \frac{1-\mathrm{Pr}}{2}(\gamma-1)M_\infty^2 \frac{\partial}{\partial y}(u^2)\right] \\
k_s &= \frac{1}{\rho_s}, \qquad \sigma_s = \frac{\mathrm{Pr}}{\mu_s}.
\end{aligned}
\tag{3}
$$

Here β is the shock wave inclination angle, γ is the free-stream ratio of specific heats, H is the total enthalpy and the subscript s indicates the flow parameters behind the shock wave.

It is shown in the paper by Cheng (1994) that for a flat plate with zero and small angles of attack, within the framework of the models of thin and full viscous layers, the effects of the shock wave structure and corrections for viscous stress on the shock wave are small and can be ignored in the basic approximation. Indeed, a comparison of the present calculations with the results obtained under inviscid conditions on the shock wave showed that the difference in Stanton numbers is less than 3%.

2.3. Initial conditions and algorithm of calculation

To solve the system of equations (2), one has to set the initial conditions at a certain value $x = x_0$. The estimates of the Knudsen number $\mathrm{Kn}_x = M_\infty C/\mathrm{Re}_x$ (as in Metcalf et al. (1969) and Pan and Probstein (1966)) obtained in the present calculations showed that its value is of the order of 10^{-3}. This testifies that the continuum condition is satisfied.

The analysis of the experimental data of McCroskey et al. (1966), Harbour and Lewis (1967), Nagamatsu et al. (1961), McCroskey and McDougall (1966) showed that the viscous flow fills the whole region between the plate surface and the undisturbed flow in the vicinity of the sharp leading edge at the end of the merged layer region and in the beginning of the region of strong shock wave/boundary layer interaction, and there is no explicit inviscid flow in this region. It is assumed, therefore, that the flow in the initial cross-section can be described by the boundary layer equations and that the shock wave is straight between the leading edge of the plate

and this cross-section. These assumptions can induce a certain error in the solution used as initial conditions. However, due to the parabolicity of the FVSL equations, the error die out soon downstream. For $x = x_0$ the system of FVSL equations (2) can be reduced to ordinary differential equations using the transformation $\xi = x$, $\eta = y\sqrt{\mathrm{Re}_L}/\sqrt{x}$ typical of boundary layer flows with a uniform external flow.

The viscous shock layer equations (2) are then solved with respect to the x coordinate using the marching method. Nonlinearity of this system of equations requires an iteration approach which allows one to reduce the problem within one iteration to a sequential solution of difference boundary-value problems approximating equations (2):

$$A_n W_{n+1} + B_n W_n + C_n W_{n-1} + D_n = 0,$$

where n is the number of node of the difference grid with respect to the y coordinate. The parameter W stands for both the velocity components, temperature, or density. The boundary conditions on the body are obtained by writing the slip and temperature drop conditions in terms of one-side differences for three points. We also add the condition $\dfrac{\partial P}{\partial y} = 0$ on the body surface, from which we obtain an additional condition for density using the equation of state. The conditions on the shock wave are reduced now to equality $W = 1$ for all parameters.

Strictly speaking, this problem is not correct, since system (2) is not strictly parabolic, and disturbances can be transported upstream by the subsonic part of the boundary layer. Some regularization is needed to suppress these disturbances. The method of the present study is based on the idea of the "sublayer aproximation" of Lin and Rubin (1973) that the term $\dfrac{\partial P}{\partial x}$ is calculated outside the subsonic region and is used there as a constant quantity.

The iteration process in each cross-section continues until the condition of the massflow conservation when passing through the shock wave is satisfied:

$$\int_0^{y_s(x)} \rho u dy|_x = \int_0^{y_s(x)} \rho u dy|_{x=x_0} + \int_{x_0}^{x} \frac{\sin(\beta+\alpha)}{\cos\beta} dx. \tag{4}$$

The solution yields the velocity, temperature, density and pressure profiles in the whole shock layer, as well as the shock wave position. These data were used to calculate the skin friction coefficient on the plate surface and the heat transfer coefficient St (Stanton number) which, under the slip boundary conditions, takes into account the "slipping-friction" energy transfer (Rudman and Rubin, 1968):

$$St = \left(k\frac{\partial T}{\partial y} + u\mu\frac{\partial u}{\partial y}\right)\Big|_{y=0} / \rho_\infty U_\infty (H_\infty - H_w).$$

Since the FVSL equations are similar to the compressible boundary layer equations, a two-layer implicit difference scheme with weights of the second-order accuracy in both directions, previously used in Vetlutsky and Poplavskaya (1982), was chosen to solve them. The FVSL computations were performed on a difference mesh with 400 points along the normal, x-step equal to 0.0001, slip and accommodation coefficients $\alpha_u = \alpha_T = 0.8$ (Lengrand et al., 1992), $\mathrm{Pr} = 0.7$, $\gamma = 1.4$. Viscosity was approximated by Sutherland's function from Abramovich (1969).

3. Experimental technique

The measurements were taken in the hypersonic nitrogen wind tunnel T-327 based at ITAM SB RAS (Drucker et al., 1975) for a Mach number $M_\infty = 21$ and unit Reynolds number based on the free stream

parameters $Re_1 = 6 \times 10^5$ m^{-1}, stagnation pressure $P_0 = 8$ MPa, stagnation temperature $T_0 = 1100$ K, and with a uniform flow core diameter of 0.1 m. Flow visualization and the mean density distribution using electron-beam fluorescence were obtained. For this purpose, the wind tunnel is equipped with an electron gun generating a probing beam with diameter of 1 mm and energy of 12-15 keV. Heat fluxes to the plate surface were measured by calorimetric gages and an IR imaging system.

A tapered plate model made of blackened aluminium with 0.1 m leading edge width, 0.06 m trailing edge width, 0.2 m length, and 0.008 m thickness was used for electron-beam measurements. The front part of the plate was a 7 degree wedge, the leading edge bluntness being less than 0.05 mm. The side edges of the plate were made as 20 degree wedges. During the experiment the plate temperature varied within 290-320 K as a result of its heating by the flow. The angle of attack of the plate could be varied between $-10°$ and $+17°$. A plate 0.35 m long, other dimensions being equal to the above model, was also used for electron-beam visualization of the flow. It use was restricted to angles of attack within 0 and $+5°$ because of strong flow blockage.

A steel plate with 0.01 m thickness, 0.34 m length, 0.08 m leading edge width, and 0.05 m trailing edge width was used for heat flux measurements. The leading and side edges of the plate model were scarfed at an angle of 11°, the leading edge bluntness being 0.05 mm. For heat flux measurements, an insert made of heat-insulating material with 0.307 m length, 0.012 m width, and 0.006 m thickness was placed at the model axis. Five calorimetric gages were mounted along the insert centerline at distances of 0.03, 0.06, 0.09, 0.15, and 0.27 m from the leading edge of the plate. The calorimetric gages were copper cylinders 1.9 mm in diameter and 1.7 mm long with thermocouples caulked into them and mounted flush with the heat insulator surface. The plate model was installed on a rotating device that allowed for its positioning at angles of 0 to $+5°$.

The fluorescence of long-living electron states of nitrogen molecules ($> 10^{-5}$ s) induced by inelastic collisions with a beam of fast electrons was used for the flow visualization on the plate. The electron-beam visualization clearly reveals the shock wave structure but gives only a qualitative picture of density distribution.

The quantitative information about the density distribution in the flow on a plate was obtained by registration of the fluorescence of short-living (6×10^{-8} s) states of nitrogen molecules and molecular ions. A linear relation was observed between the gas density in the measurement point and fluorescence intensity for densities not larger than 3×10^{21} m^{-3}. For conditions of the present experiment, the gas density in the shock wave reaches values of 3.5×10^{22} m^{-3}, and this relation is no longer linear, mainly because of the electron beam scattering and additional excitation of fluorescence by secondary electrons. Starting at gas densities of 2×10^{22} m^{-3}, some effect is exerted by the process of excitation quenching in intermolecular collisions. The influence of the first two factors was taken into account by constructing a calibration curve establishing a relation between the local gas density and fluorescence intensity (Vetlutsky et al., 1995). This approach for density recovery from fluorescence intensity is valid only for two-dimensional plane flows, which is just the case for a flow on a plate (Vetlutsky et al., 1995).

Details of the optical system for fluorescence intensity registration can be found in Maslov et al. (1996a). The spatial resolution was 1.7 mm along the plate and 10 mm across the plate. In the direction normal to the shock layer the spatial resolution was substantially dependent on the density at the measurement point. Thus, for density values lower than or equal to the free stream density, the spatial resolution near the plate surface was close to the initial electron beam diameter (1 mm). In the high-density region adjacent to the shock wave, the spatial resolution decreases as the electron beam expands and reaches 3 mm at the maximum density. Measurements in practice showed that it is not possible to resolve the fine structure of the layer in the shock wave region without a procedure for deconvolution of the measurement data. This was not done in the present study, which increased the error of density measurements in this region.

The model surface temperature was measured by a module optical-mechanical scanning IR imaging system TB-M3 developed at ITAM (Bashurov et al., 1986). To gain a better accuracy of measurement, the IR imaging system worked in a line (one-dimensional) scanning regime. The temperature was calculated using a calibration dependence of the Plank function type obtained experimentally for a reference radiator: $I = A/(e^{B/T} - 1)$, where I is the IR system signal, A and B are calibration constants.

The measurement results were processed using the technique described in Maslov et al. (1996b). The technique is based on the finite-difference calculations of one-dimensional unsteady differential equations of heat conduction in a coordinate system fixed at the model surface. This approach takes into account the surface curvature, the longitudinal heat overflow and does not require knowledge of the recovery temperature.

4. Discussion of results

To verify the algorithm used in solving the FVSL equations for a plate at incidence, the results were compared with experimental data obtained by the authors and found in other papers. A good agreement was obtained for the following parameters:

1) shock wave position (comparison with the data of McCroskey et al. (1966), Shorenstein and Probstein (1968)) in Poplavskaya and Vetlutsky (1997) and Vetlutsky et al. (1997);
2) shock wave intensity, i.e. $\rho_{\max}/\rho_\infty$ (comparison with the universal curve from Metcalf et al. (1969)) in Poplavskaya and Vetlutsky (1997);
3) velocity profiles (comparison with theoretical data of Hantzsche and Wendt from Loitsyansky (1973) at $M_\infty = 5$ and experimental data obtained from Pitot measurements at $M_\infty = 6$) in Poplavskaya and Vetlutsky (1997) and Maslov et al. (1996a);
4) density profiles (comparison with experimental data of McCroskey et al. (1966) for the transitional region between the merged layer and the strong interaction region) at $M_\infty = 24.5$ in Poplavskaya and Vetlutsky (1997).

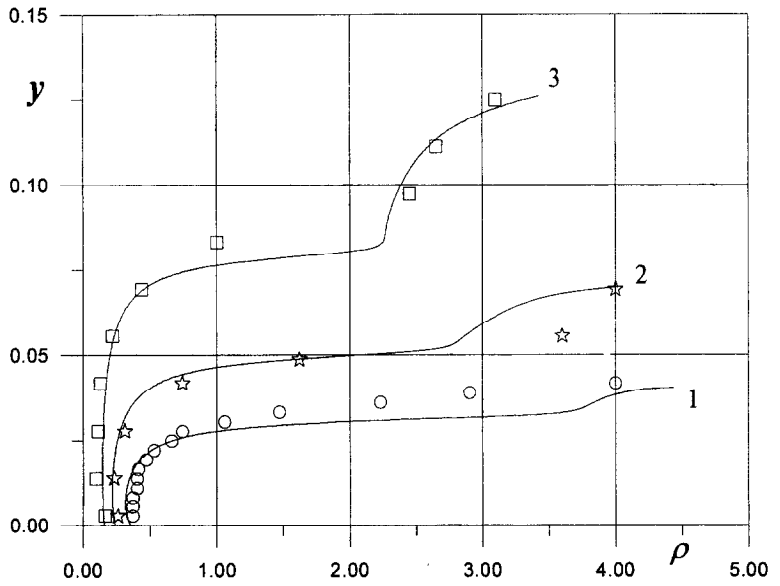

Fig. 1. – Comparison of calculated and experimental density profiles for $Re_1 = 6 \times 10^5$ m^{-1}, $L = 360$ mm, $M_\infty = 21$, $T_0 = 1100$ K, $T_w = 290$ K, $\alpha = 0°$ in different cross-section: 1 – $x = 0.22$; 2 – $x = 0.4$; 3 – $x = 0.81$.

Multiple measurements of density in hypersonic flow ($M_\infty = 21$) past a plate were performed using the above technique. The experimental data obtained (density versus the normal coordinate) are shown by points in figure 1. Lines 1-3 (results of FVSL computations) correspond to the cross-sections $x = 0.22$, 0,4, 0.81. The agreement of calculated and experimental data is satisfactory practically over the entire region under consideration. A slight discrepancy near the shock wave can be explained, on one hand, by the fact the shock wave is treated as a discontinuity in the computational model. On the other hand, as described above, the error of experimental values of density increases near the shock wave because of primary electron scattering and a larger region of secondary fluorescence.

Figure 2 shows the density profiles normal to the body for different angles of attack. It is seen that as the angle of attack increases, the density increases at smaller distances between the body and the shock wave. A comparison of experimental and calculated density profiles in the cross-section $x = 0.417$ (100 mm) for angles of attack $\alpha = 0°$ and $+10°$ is shown in the same figure. The agreement of calculated and experimental data is satisfactory practically in the entire shock layer (the error of experimental values of density is shown in figure 2).

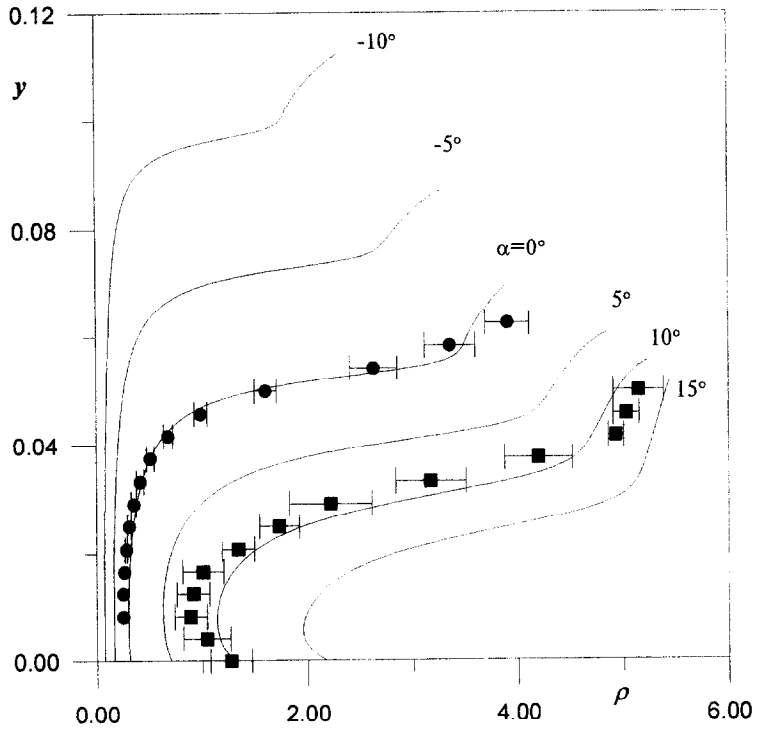

Fig. 2. – Experimental and calculated density profiles: $\mathrm{Re}_1 = 5.8 \times 10^5$ m^{-1}, $M_\infty = 21$, $T_0 = 1150$ K, $T_w = 299$ K, $L = 240$ mm, $x = 0.417$, ● $-\alpha = 0°$, ■ $-\alpha = +10°$.

The shock wave position in the flow past a plate at zero incidence determined from the electron-beam flow visualization photographs (circles), measured by a Pitot probe (triangles) and schlieren technique (dash-dots) from Hillard et al. (1971) is shown in figure 3. The solid line indicates the shock wave position determined by solving the FVSL equations using the algorithm suggested in the present paper.

Figure 4 shows the shock wave position as a function of the angle of attack α in different x cross-sections. The calculated data are indicated by solid lines 1-3 ($x = 0.8$, 0.5, and 0.417, respectively), the symbols denote the experimental data obtained by the authors using the electron-beam technique. It is seen that the shock wave stand-off distance at a given cross-section decreases as the angle of attack increases, and a certain minimum is observed at $\alpha \approx 15°$.

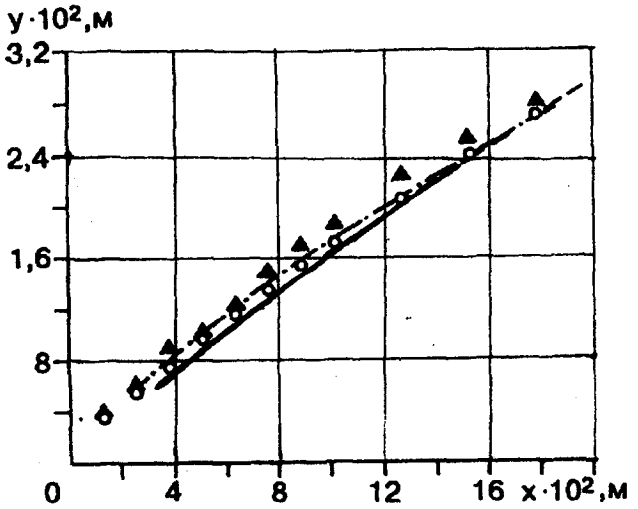

Fig. 3. – Comparison of the calculated shock wave position with experimental data of Hillard et al. (1971) for $\alpha = 0°$, $\mathrm{Re}_L = 2.52 \times 10^5$, $L = 0.2$ m, $M_\infty = 19$, $T_0 = 1650$ K, $T_w = 544.5$ K.

McCroskey et al. (1967) present a universal dependence of the shock wave position $y_s/\alpha x$ on the parameter $\overline{\chi}/(M_\infty \alpha)^2$ where $\overline{\chi} = M_\infty^3 \sqrt{C}/\sqrt{\mathrm{Re}_x}$. It is shown there that experimental data in the merged layer region for a wedge and a plate at an incidence angle of 2° are in satisfactory agreement with Cheng's theory of strong

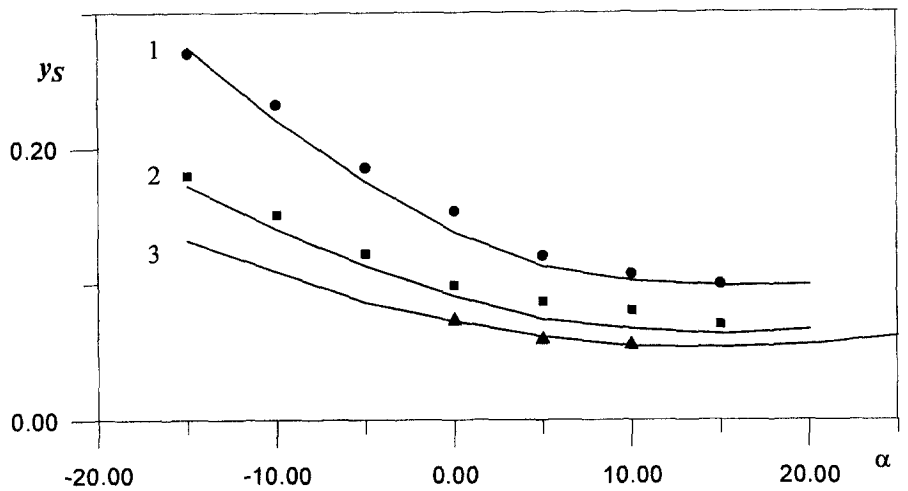

Fig. 4. – Shock wave position in plate cross-sections versus the angle of attack for $M_\infty = 21$:
1, ● – $\mathrm{Re}_1 = 6 \times 10^5$ m^{-1}, $x = 0.8$, $L = 200$ mm, $T_0 = 1100$ K, $T_w = 310$ K;
2, ■ – $\mathrm{Re}_1 = 6 \times 10^5$ m^{-1}, $x = 0.5$, $L = 200$ mm, $T_0 = 1100$ K, $T_w = 310$ K;
3, ▲ – $\mathrm{Re}_1 = 5.8 \times 10^5$ m^{-1}, $x = 0.417$, $L = 240$ mm, $T_0 = 1150$ K, $T_w = 299$ K.

interaction (Cheng et al., 1961). The results of the present calculations (solid curves) are compared in figure 5 with the universal dependence from Cheng et al. (1961) (dashed curve):

$$\frac{y_s}{\alpha x} = 1.21\sqrt{\frac{\gamma-1}{\gamma+1}\left(0.664+1.73\frac{T_w}{T_0}\right)}\sqrt{\frac{\overline{\chi}}{(M_\infty\alpha)^2}}.$$

Their satisfactory agreement shows that this universal dependence holds not only for the merged layer region, but also for the strong interaction region. It should be noted that the FVSL calculations underestimate the shock wave position. This is in agreement with the study of Cheng (1995).

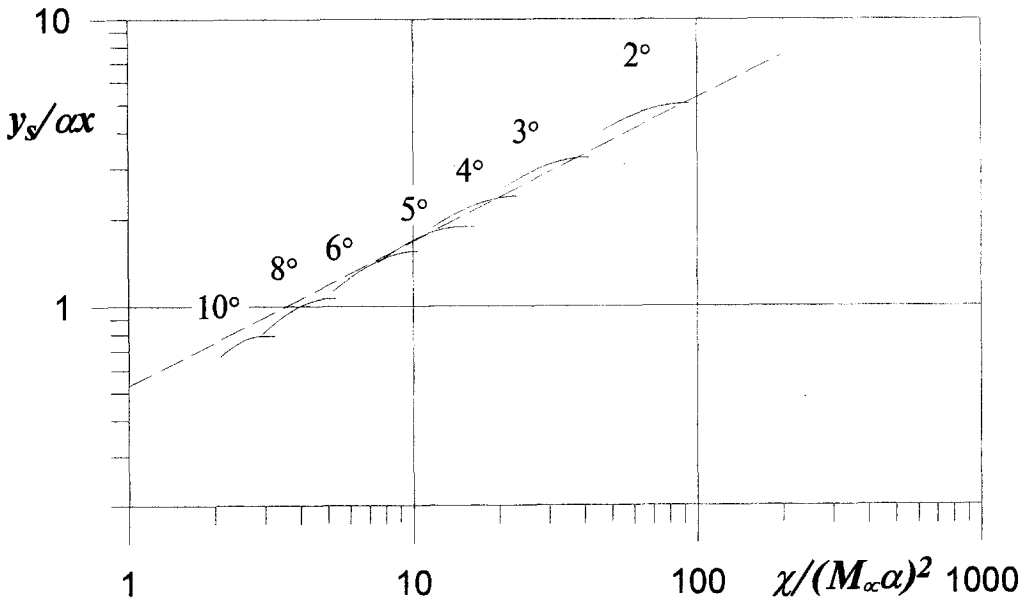

Fig. 5. – Comparison of the calculated shock wave position for angles of attack 2° to 10° with the universal curve of Cheng et al. (1961) for $M_\infty = 21$, $\mathrm{Re}_1 = 6 \times 10^5$ m^{-1}, $L = 200$ mm, $T_0 = 1100$ K, $T_w = 310$ K.

Figure 6 from Wallace and Burke (1965) shows a comparison of Stanton numbers measured by different authors and the calculated data (solid curves) for various flow regimes past a plate. The temperature factor is smaller than 0.1 everywhere. It is seen that the maximum difference is 35%, and the curve for the strong interaction region follows the lower boundary of experimental data. Note that the formula for the heat flux of Cheng (1961) coincides with this curve. The FVSL results for conditions 1, 2, 3 (see the figure) are presented in the graph by the corresponding curves. The dashed curve in the same figure shows the theoretical results of Pan and Probstein (1966).

Note that the calculation results depend strongly on the Reynolds number. In the present work ρ_∞ and U_∞, which were used for the Reynolds number calculations $\mathrm{Re}_L = \rho_\infty U_\infty L/\mu_\infty$, were found from isentropic formulas taking into account the influence of vibrational degrees of freedom. Viscosity μ_∞ at temperature T_∞ lower than 120 K was determined from the linear law, while for $T_\infty > 120$ K from the Sutherland law. Possibly, this method of calculating Re_L does not coincide with the Reynolds number calculation by Wallace and Burke (1965).

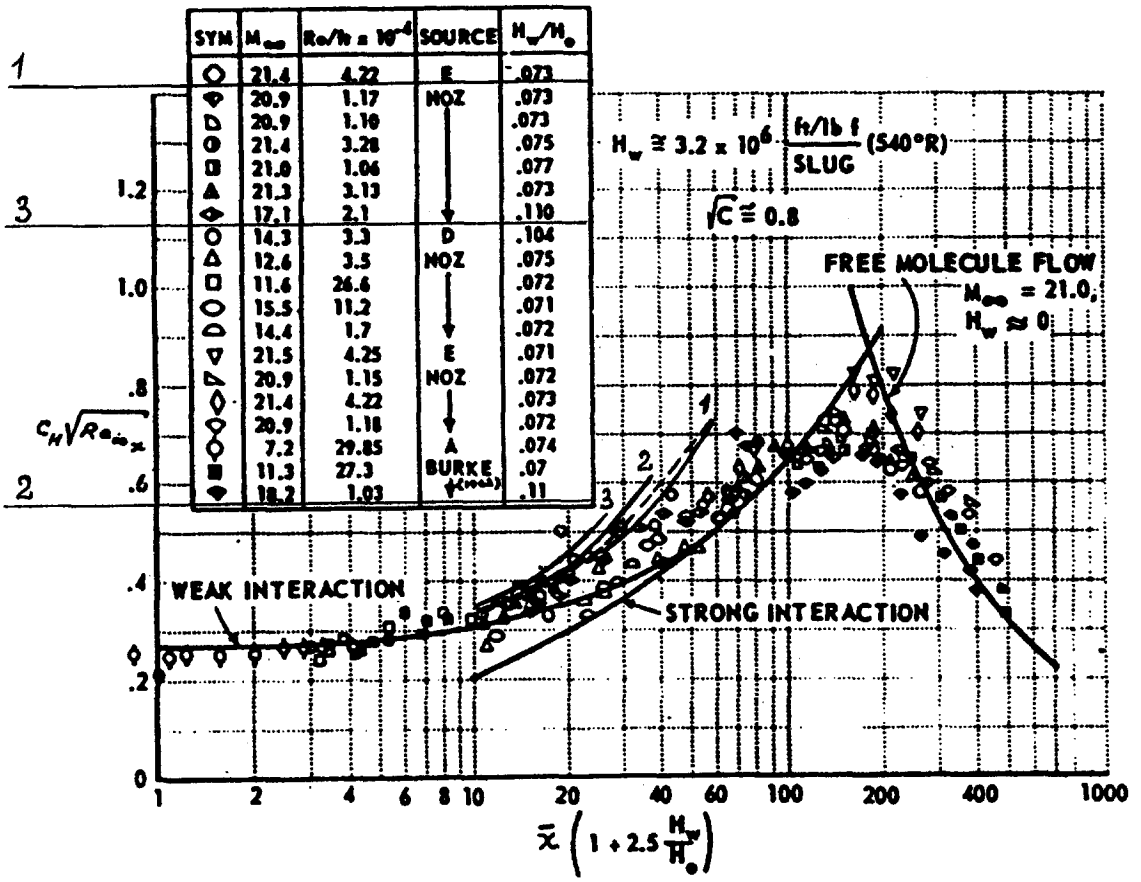

Fig. 6. – Comparison of the FVSL calculations with experimental and theoretical data of other authors on the heat flux (see Wallace and Burke (1965)).

Figure 7 shows a comparison of calculated and experimental values of the Stanton number for angles of attack $\alpha = 0°$ (Fig. 7a) and 5° (Fig. 7b). The solid lines 1 correspond to calculations on the basis of the FVSL equations with the shock wave position determined from experimental results. The solid curves 2 correspond to the FVSL computations with the shock wave position which is calculated from the condition of constant flow rate when passing through the shock wave (4). Here the triangles indicate the experimental data obtained using the IR imaging system, while the exprimental data obtained from calorimetric gages are shown by circles and rhombi. The Stanton number error determined by the IR imaging system is shown in figure 7. It is mainly caused by the error of the model surface temperature measurement and by the uncertainty of heat insulating material characteristics. The calculated data lie within this error, which testifies to their reliability. As was predicted by the strong interaction theory of Pan and Probstein (1966), the values of St are inversely proportional to $x^{3/4}$ rather than to $\sqrt{x}$, as predicted by the classical boundary layer theory.

It should be noted that experimental and theoretical data in figure 7 are presented for a large temperature factor $T_w/T_0 = 0.26$. The experimental data in figure 6 correspond to the temperature factor < 0.1. The influence of this factor was studied by Maslov et al. (1999). It is shown that St decreases as the temperature factor decreases.

Figure 8 demonstrates the applicability of the FVSL model for the Stanton number calculations versus the Reynolds and Mach numbers.

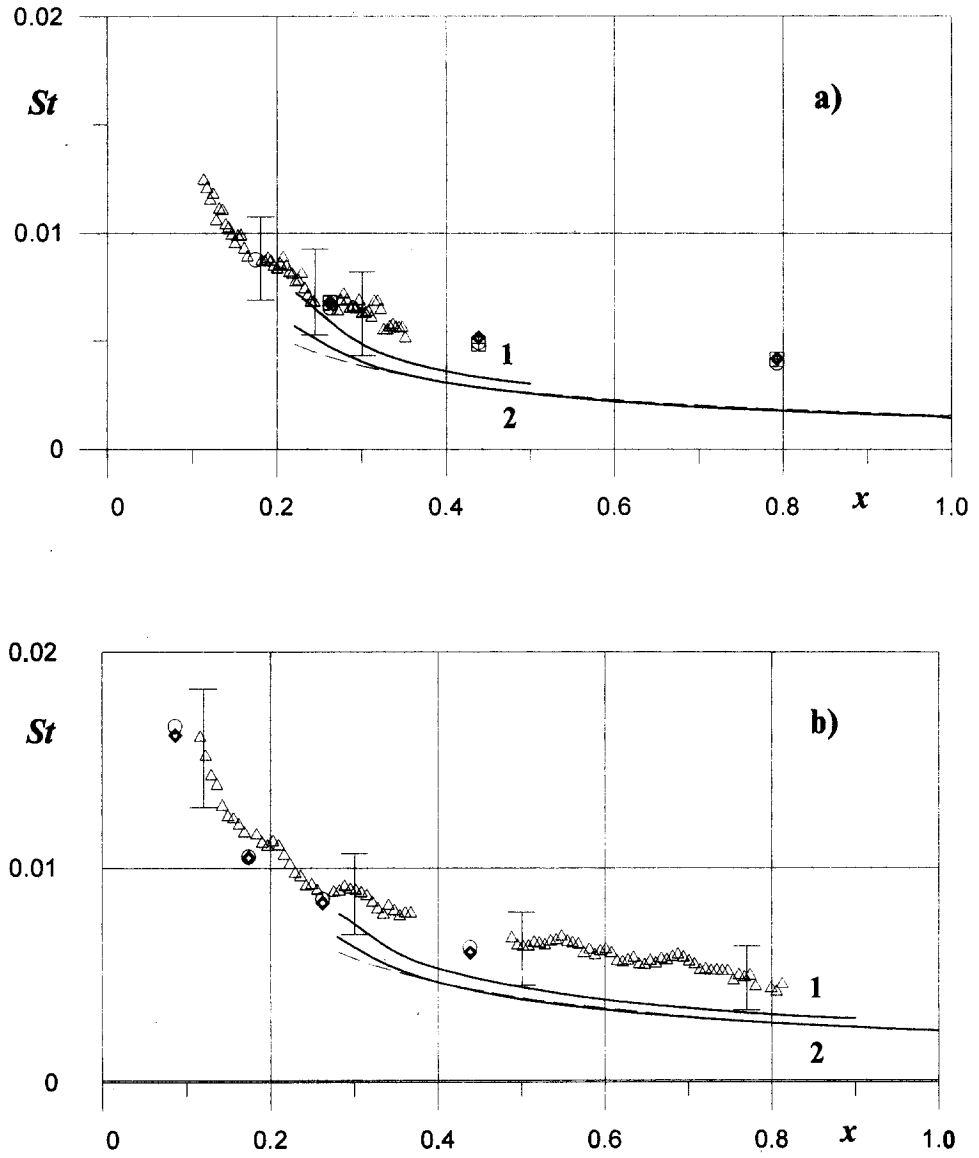

Fig. 7. – Comparison of calculated and experimental Stanton numbers for $M_\infty = 21$, $\mathrm{Re}_L = 1.93 \times 10^5$, $T_0 = 1100$ K, $T_w = 291$ K, $\alpha = 0°$ to $5°$: — - FVSL calculation, △ $-St$ (IR imaging method), ○, ◊, □ $-St$ (calorimetric gages) see approximation formula (5).

Using the above algorithm of the FVSL equations and obtaining the shock wave position from the condition of constant flow rate, we performed parametric calculations over a wide range of governing parameters: $15 \leq M_\infty \leq 25$, $\mathrm{Re}_x = 10^4$ to 10^6, $\alpha = 0°$ to $+15°$, $0.05 \leq T_w/T_0 \leq 0.26$. When analyzing the parametric FVSL computations, we obtained an empirical function approximating the results for the heat transfer coefficient:

$$St_{FVSL} = (0.016\alpha + 0.16)[M_\infty \sqrt{C}/\sqrt{\mathrm{Re}_x}]^{3/2} \tag{5}$$

(α is taken in degrees). The accuracy of approximation of the heat transfer coefficient reaches 10% on most of the plate. The Stanton numbers calculated using the approximation formula (5) are shown by the dashed curve in figure 7. It is seen that the difference lies within the above mentioned limits.

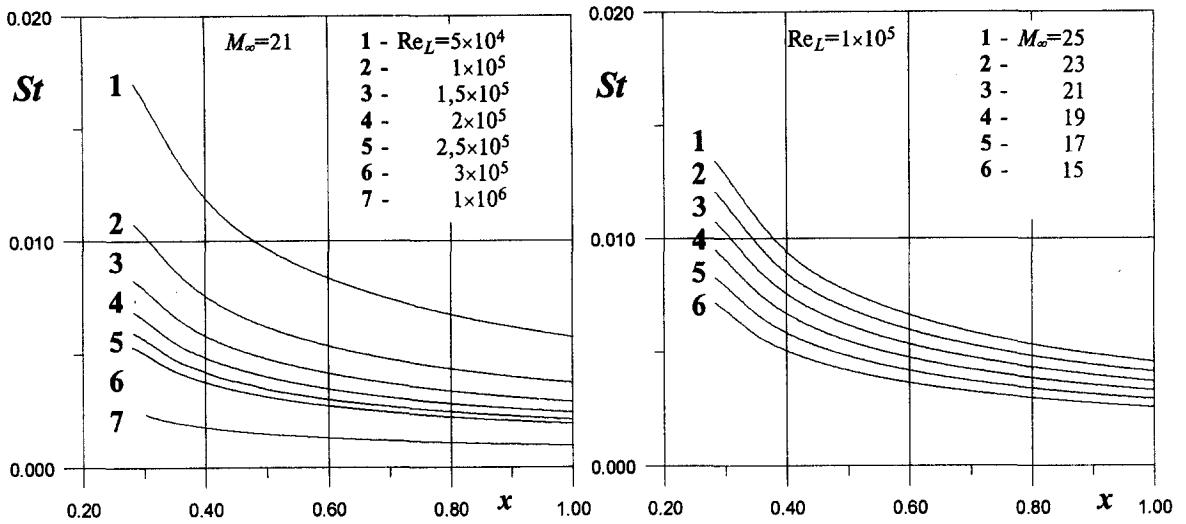

Fig. 8. – Stanton numbers versus the Reynolds and Mach numbers for $T_0 = 1100$ K, $T_w = 291$ K, $\alpha = 5°$.

5. Conclusion

1. The parametric studies performed showed that the FVSL model gives a good description of hypersonic flow past a plate both at high ($\mathrm{Re}_x \sim 10^6$) and moderate ($\mathrm{Re}_x \sim 10^4$) Reynolds numbers in a wide range of Mach numbers (15-25). The agreement between the calculated and experimental data is a serious argument in favour of the plausibility of the flow model chosen and algorithm constructed.

2. An empirical function approximating the results for the heat transfer coefficient is obtained. The accuracy of approximation reaches 10%.

Acknowledgments

The work was supported by the Russian Foundation of Basic Research (grant 98-01-00735).

REFERENCES

ABRAMOVICH G.N., 1969, Applied Gas Dynamics, Nauka, Moscow.

BASHUROV V.V., BOICHUK L.N., VORONTSOV S.S., VYSHENKOV Yu.I., 1986, Modular measurement IR imaging system TV-M, *Teplovidenie, No. 6, (Collection of papers of Moscow Institute of radio engineering, electronics and automation).*

BORODIN A.I., PEIGIN S.V., 1992, Method of global iterations for solving three-dimensional viscous shock layer equations, *High Temp.*, **30**, 1124–1129.

CHENG H.K., 1961, Hypersonic shock-layer theory of the stagnation region at low Reynolds number, Heat Transfer and Fluid Mechanics Institute, Stanford Press, Stanford, Calif., 161–175.

CHENG H.K., GORDON HALL J., GOLIAN T.C., HERTZBERG A., 1961, Boundary-layer displacement and leading-edge bluntness effects in high-temperature hypersonic flow, *J. Aerospace Sciences*, **28**, 353–381.

CHENG H.K., 1994, The viscous shock layer problem revisited, *Book Abstracts Inter. Conf. Fundamental research in aerospace science, Central Aerohydrodynamic Institute Press, Sec. 3, Zhukovsky, Russia*, 6–9.

CHENG H.K., EMMANUEL G., 1995, Perspective on Hypersonic Nonequilibrium Flow, *AIAA J.*, **33**, 385–400.

DAVIS R.T., 1970, Numerical solution of the hypersonic viscous shock-layer-equations, *AIAA J.*, **8**, 843–851.

DRUKER I.G., ZHAK V.D., SAPOGOV B.A., SAFRONOV Yu.A., 1975, Characteristics of hypersonic nitrogen wind tunnel T327 of ITAM SB RAS, *Problems of gas dynamics*, Novosibirsk, ITAM SB RAS, No. 5.

HARBOUR P.J., LEWIS J.N., 1967, Preliminary measurements of the hypersonic rarefied flow on a sharp flat plate using an electron beam probe, *In Rarefied Gas Dynamics* (ed. C.L. Brundin), **2**, 1031–1046.

HILLARD E.M. Jr., HARVEY D.W., EMORY M.L., 1971, Measurements of shock wave location in hypersonic nitrogen flow, *J. Spacecraft*, **8**, 1004–1006.

LENGRAND J.C., ALLEGRE J., CHPOUN A., RAFFIN M., 1992, Rarefied hypersonic flow over a flate plate with a sharp leading edge: DSMC, Navier-Stokes and experimental results, *8-th Intern. Symp. on Rarefied Gas Dynamics*, Vancouver.

LIN T.C., RUBIN S.G., 1973, Viscous flow over a cone at moderate incidence, *J. Computer and Fluids*, **1**, 37–57.

LOITSYANSKY L.G., 1973, *Fluid Mechanics*, Nauka, Moscow.

MAGOMEDOV K.M., 1970, Viscous hypersonic flow around blunt bodies, *Izv. AN SSSR, MZhG*, No. 2, 45–56.

MASLOV A.A., MIRONOV S.G., SHIPLYUK A.N., 1996a, An experimental study of density fluctuations in hypersonic shock layer on a flat plate, *J. Appl. Mech. Tech. Phys.*, **37**, 51–61.

MASLOV A.A., SAPOGOV B.A., SHIPLYUK A.N., 1996b, A technique for the heat flux determination in an aerodynamic experiment, *Thermophysics and Aeromechanics*, **3**, 157–164.

MASLOV A.A., MIRONOV S.G., POPLAVSKAYA T.V., VETLUTSKY V.N., 1998, On effect of the angle of attack on hypersonic flow over a plate, *High Temp.*, **36**, 754–760.

MASLOV A.A., MIRONOV S.G., POPLAVSKAYA T.V., SHIPLJUK A.N., VETLUTSKY V.N., 1999, The study of aerodynamic heating of the plate in a viscous hypersonic flow, *High Temp.* (in press).

MCCROSKEY W.J., BOGDONOFF S.M., MCDOUGALL J.G., 1966, An experimental model for the sharp flat plate in rarefied hypersonic flow, *AIAA J.*, **4**, 1580–1587.

MCCROSKEY W.J., MCDOUGALL J.G., 1966, Shock wave shapes on a sharp flat plate in rarefied hypersonic flow, *AIAA J.*, **4**, 184–186.

MCCROSKEY W.J., BOGDONOFF S.M., GENCHI A.P., 1967, Leading edge flow studies of sharp bodies in rarefied hypersonic flow, *In Rarefied Gas Dynamics* (ed. C.L. Brundin), **2**, 1047–1066.

METCALF S.C., LILLICRAP D.C., BERRY C.J., 1969, A study of the effect of surface temperature on the shock-layer development over sharp-edged shapes in low-Reynolds-number high-speed flow, *In Rarefied Gas Dynamics* (ed. L. Trilling and H.Y. Wachman), **1**, 619–634.

NAGAMATSU H.T., SHEER Jr. R.E., SCHMID J.R., 1961, Flow around the plate by the hypersonic flow of rarefied gas at high temperatures, *ARS J.*, **31**, 902–910.

PAN Y.S., PROBSTEIN RONALD F., 1966, Rarefied-flow transition at a leading edge, *In Fundamental phenomena in hypersonic flow* (ed. J. Gordon Hall), 259–306.

POPLAVSKAYA T.V., VETLUTSKY V.N., 1997, A numerical study of viscous shock layer on a plate, *J. Appl. Mech. Tech. Phys.*, **38**, 91–100.

RUDMAN S., RUBIN S.G., 1968, Hypersonic viscous flow over slender bodies with sharp leading edges, *AIAA J.*, **6**, 1883–1890.

SHORENSTEIN M.L., PROBSTEIN R.F., 1968, The hypersonic leading-edge problem, *AIAA J.*, **6**, 1898–1906.

TIRSKY G.A., 1975, On the theory of hypersonic viscous chemically reactive gas flow over plane and axisymmetric blunted bodies with injection, *Papers of the Institute of Mechanics of Moscow State University*, No. 39, 5–38.

TIRSKY G.A., UTYUZHNIKOV S.V., 1989, Comparison of thin and full viscous shock layer models in the problem of supersonic viscous flow around blunted cones, *Prikl. Mat. Mekh.*, **53**, 963–969.

VERSHININ I.V., TIRSKY G.A., UTJUZHNIKOV S.V., 1991, Supersonic laminar flow over the windward side of infinite-span swept wings in a wide range of Reynolds numbers, *Izv. AN SSSR, Mekhanika zhidkosti i gaza*, No. 4, 40–44.

VETLUTSKY V.N.POPLAVSKAYA T.V., 1982, On calculating the laminar boundary layer on a flat triangular plate with supersonic leading edges, *Numerical methods of continuum mechanics*, **13**, 31–43.

VETLUTSKY V.N., MASLOV A.A., MIRONOV S.G., POPLAVSKAYA T.V., SHIPLYUK A.N., 1995, Hypersonic flow on a flat plate. Experimental results and numerical simulation, *J. Appl. Mech. Tech. Phys.*, **36**, 60–67.

VETLUTSKY V.N., MIRONOV S.G., POPLAVSKAYA T.V., 1997, Hypersonic flow over a plate at incidence, *Thermophysics and Aeromechanics*, **4**, 33–39.

VORONKIN I.G., 1974, Calculation of viscous layer on blunted cones, *Izv. AN SSSR, Mekhanika zhidkosti i gaza*, 99–105.

WALLACE J.E., BURKE A.F., 1965, An experimental study of surface and flow field effects in hypersonic low density flow over a flat plate, *In Rarefield Gas Dynamics* (ed. J.H. de Leeww), **1**, 487–507.

(Manuscript received December 18 1997;
revised and accepted July 2 1998.)